

Hydroxyapatite-dextran methacrylate core/shell hybrid nanocarriers for combinatorial drug therapy

S. Ram Prasad^{1,2} , A. Jayakrishnan^{1,a),c)}, T. S. Sampath Kumar^{2,b)}

¹Biomaterials Laboratory, Department of Biotechnology, Bhupat and Jyoti Mehta School of Biosciences, Indian Institute of Technology Madras, Chennai 600 036, Tamil Nadu, India

²Medical Materials Laboratory, Department of Metallurgical and Materials Engineering, Indian Institute of Technology Madras, Chennai 600 036, Tamil Nadu, India

^{a)}Address all correspondence to these authors. e-mail: jayakrishnan1953@gmail.com; jayakrishnana@rgcb.res.in

^{b)}e-mail: tssk@iitm.ac.in

^{c)}Present address: Raja Ramanna Fellow, Rajiv Gandhi Centre for Biotechnology, Jagathy, Trivandrum 695 014, Kerala, India

Received: 2 April 2020; accepted: 6 July 2020

In this study, a hybrid dual drug-loaded hydroxyapatite-oxidized dextran methacrylate core-shell nanocarrier was formulated and explored for combinatorial delivery of doxorubicin (DOX) and methotrexate (MTX) to bone cancer. The synthesized nanocarrier was well characterized by different techniques. *In vitro* drug release studies in both acidic (pH 5) and alkaline (pH 7.4) conditions showed sequential release of MTX followed by DOX in a sustained manner for 10 days. Biocompatibility and cytotoxicity studies performed using drug-loaded nanoparticles (NPs) on fibroblast L929 cells and osteosarcoma MG63 cells (OMG63) showed that the NPs were highly biocompatible and showed concentration-dependent toxicity. Gene expression studies in OMG-63 cells exhibited the upregulation of caspase-3 and BAX which confirmed the apoptosis induced by dual drug-loaded NPs. The nanocarrier is expected to be a potential bone void filling material, as well as a platform for sequential delivery of DOX and MTX for the treatment of bone cancer.

Introduction

Bone cancer is a malignant tumor which originates in the bone and destroys the healthy bone tissues. Bone cancer is a dangerous disease which can spread to distant organs easily and bone is a common site to be affected by metastatic cancer [1, 2]. Bone metastases are the main cause of morbidity and mortality in patients with advanced malignant diseases [3, 4, 5]. Among the 45 different types of bone tumors, osteosarcoma is the most common and important primary bone tumor (31.5%) followed by chondrosarcoma, Ewing's sarcoma and chondroma [6, 7].

The treatment of bone cancer involves surgery, fixation, radiotherapy and systemic chemotherapy before and after surgery [8, 9]. Among the different types of treatment, chemotherapy is an essential requisite but repeated usage of single chemotherapeutic agents involving high doses leads to adverse effects, such as systemic toxicity and multidrug resistance. Combination therapy of multiple chemo drugs enhances treatment efficacy by acting on multiple pathways with synergistic effects [10, 11].

Nanotechnology-based combination therapy with nanocarriers, such as dendrimers, liposomes, carbon nanotubes,

polymer drug conjugates, micelles, and polymeric, inorganic and ceramic nanoparticles (NPs) has gained considerable attention [11, 12, 13, 14, 15, 16]. Combined delivery of drugs using nanocarriers has the advantage of protecting the drugs from degradation in the reticuloendothelial system thereby enabling high concentration of drugs at the target site with reduced toxic effects and with much lower doses [6, 11, 12]. Significant anti-tumor effect was observed by using NPs as carrier with or without the combination of other therapies, such as radiotherapy, hormone and immunotherapy [7, 11].

Hydroxyapatite (HA)-based nanocarrier has attracted much attention for the treatment of bone cancer, due to its chemical/compositional similarity with the bone mineral, as well as its ability to deliver the drugs in a sustained manner through diffusion-controlled release kinetics [17, 18, 19]. HA core-shell NPs and polymer-HA-based composite nanocarriers have been widely studied as platforms for combinational therapy in the treatment of bone cancer [20, 21, 22, 23, 24]. Numerous strategies have been attempted to construct the HA core polymeric shell nanocomposite carriers. Among

them, surface modification of HA become the most promising technique in achieving core-shell architecture and unique advantages over the other systems.

Surface modification can also improve the structural integrity, interface between inorganic-organic matrices and covalent coupling of therapeutic molecules. Various approaches have been explored for the surface modification of HA using different polymers by different mechanisms [25, 26, 27, 28, 29, 30, 31]. To the best of the available literature, synthetic polymers, such as acrylics, lactides and polyethers, have been studied for grafting on HA NPs. In this study, an attempt has been made to graft the natural polysaccharide dextran onto the HA for combinatorial delivery of two chemotherapeutic drugs, such as doxorubicin (DOX) and methotrexate (MTX). Dextran is a hydrophilic polysaccharide consisting of α -1,6-linked D-glucopyranose residues and widely studied for biomedical applications due to its biocompatibility, biodegradability, hydrophilicity and target specificity [31, 32].

Dextran as a drug carrier has unique advantages, such as stability in both acidic and alkaline conditions due to glycosidic bonds and the presence of numerous hydroxyl groups in the polymer facilitates derivatization and drug conjugation which protects the drug from degradation and passive targeting ability in solid tumor through enhanced permeability and retention effect [32, 33, 34, 35]. Anticancer drugs, such as daunorubicin, mitomycin, 5-fluorouracil, cisplatin, MTX and DOX, were covalently coupled to the dextran and among them, DOX showed superior anti-tumor activity with reduced toxic effects. Compared to free DOX, dextran-DOX conjugates inhibited P-glycoprotein (P-gp) pump overexpressed in multidrug-resistant cells and showed the best therapeutic effect with long survival rate in mice models [34, 35].

Dextran contains vicinal diols, which can be easily converted to aldehyde by periodate oxidation. The aldehyde groups in the oxidized dextran can be used for coupling amino groups in the therapeutic molecules via imine bond formation (Schiff base reaction) [33, 35]. In our study, we have synthesized dextran methacrylate (DEX-MA) and grafted it onto the HA NPs. Periodate oxidization of DEX-MA-grafted HA NPs created aldehyde groups in the graft polymer to which DOX was covalently conjugated through Schiff base reaction. MTX was then physically loaded onto the NPs and examined for the combinatorial delivery of two therapeutic molecules. The dual drug-loaded DEX-MA-conjugated HA NPs will act as a better bone void filling material, as well as a sustained delivery system for the treatment of bone cancer.

Results and Discussion

Characterization of NPs

FTIR spectra of grafted NPs and drug-loaded NPs are shown in Fig. 1. HA NPs showed absorption bands at 3570 cm^{-1} (Structural OH), 3445 cm^{-1} (H_2O adsorption), 1644 cm^{-1} (H_2O

adsorption), 1092 cm^{-1} (HPO_4^{2-}), 1057 cm^{-1} (PO_4^{3-} -bending), 632 cm^{-1} (structural OH), 602 cm^{-1} and 571 cm^{-1} (PO_4^{3-} -bending) [Fig. 1(a)]. DEX-MA showed prominent peaks at 3406 cm^{-1} (O-H stretching), 2930 cm^{-1} (C-H stretching), 1719 cm^{-1} (C=O stretching, ester), 1637 cm^{-1} (C=C stretching) and 814 cm^{-1} (C=C-H stretching) [Fig. 1(b)]. DM-g-HA NPs showed bands at 3571 cm^{-1} (Structural OH), 3406 cm^{-1} (OH stretching), 2928 cm^{-1} (C-H stretching), 1726 cm^{-1} (C=O ester bond of DM), 1642 cm^{-1} (C=C stretching), 1455 cm^{-1} (C-H bending), 1243 cm^{-1} (C-O stretching), 1091 cm^{-1} (HPO_4^{2-}), 1047 cm^{-1} (PO_4^{3-} -bending), 632 cm^{-1} (structural OH), 602 cm^{-1} (PO_4^{3-} -bending) [Fig. 1(c)]. The appearance of a new peak at 1627 cm^{-1} (Carboxyl stretching in oxidized dextran) in addition to all other peaks of DM-g-HA NPs confirmed the oxidation of DM [Fig. 1(d)]. DOX-conjugated oxidized dextran methacrylate (ODM)-g-HA NPs showed additional bands at 2850 , 1238 and 1282 cm^{-1} (C-N Stretching) and 1630 and 1582 cm^{-1} (C=N) [Fig. 1(e)]. The spectrum of MTX-DOX-conjugated ODM-g-HA NPs showed absorption bands at 3570 cm^{-1} (O-H stretching), 3432 cm^{-1} (N-H stretching), 2921 cm^{-1} (C-H stretching), 1630 , 1508 and 1456 cm^{-1} (aromatic C=C stretching), 1384 cm^{-1} (C-H bending) and 1159 cm^{-1} (C-N stretching) [Fig. 1(f)]. This confirmed the presence of MTX in the NPs.

The crystallinity and purity of the synthesized HA NPs and polymer-grafted NPs were characterized using XRD method and compared with standard JCPDS data (09432). Figure 2 (a) shows the diffraction pattern of HA NPs and found to be highly crystalline in nature. Figures 2(b) and 2(c) correspond to the diffraction pattern of dextran and DEX-MA which were found to be amorphous in nature. The polymer-grafted samples and drug-loaded samples DM-g-HA NPs, ODM-g-HA NPs, DOX-ODM-g-HA NPs and MTX-DOX-ODM-g-HA NPs (Figs. 2(d)–2(g)) show diffraction peaks of HA and a broad hump between 10 and 25° due to the polymer grafting and adsorption of the drug molecules.

The grafting efficacy and thermal stability of the NPs were studied using thermal analysis (TGA). HA NPs showed 1.28% weight loss due to the evaporation of water and were thermally stable up to 750°C [Fig. S1(a)]. Three-stage degradation was observed for DM-g-HA NPs with the loss of water occurring at 100°C followed by 243.6°C (88.03%) and 438.54°C (68.25%) due to the loss of grafted polymer [Fig. S1(b)]. ODM-g-HA NPs showed degradation at 107.33°C (92.75%) due to moisture loss and from 211.46°C (90.59%) to 420.19°C (59.22%) due to the degradation of polymer [Fig. S1(c)]. DOX-ODM-g-HA NPs showed a four-stage degradation starting at 106.3°C (93.75%) attributed to the loss of water, and 218.05°C (90.35%), 340.06°C (73.62%) and 471.22°C (67.50%) due to the degradation of drug and polymer [Fig. S1(d)]. In case of MTX-DOX-ODM-g-HA NPs, after water loss at 110.62°C (95.84%), two-stage degradation was

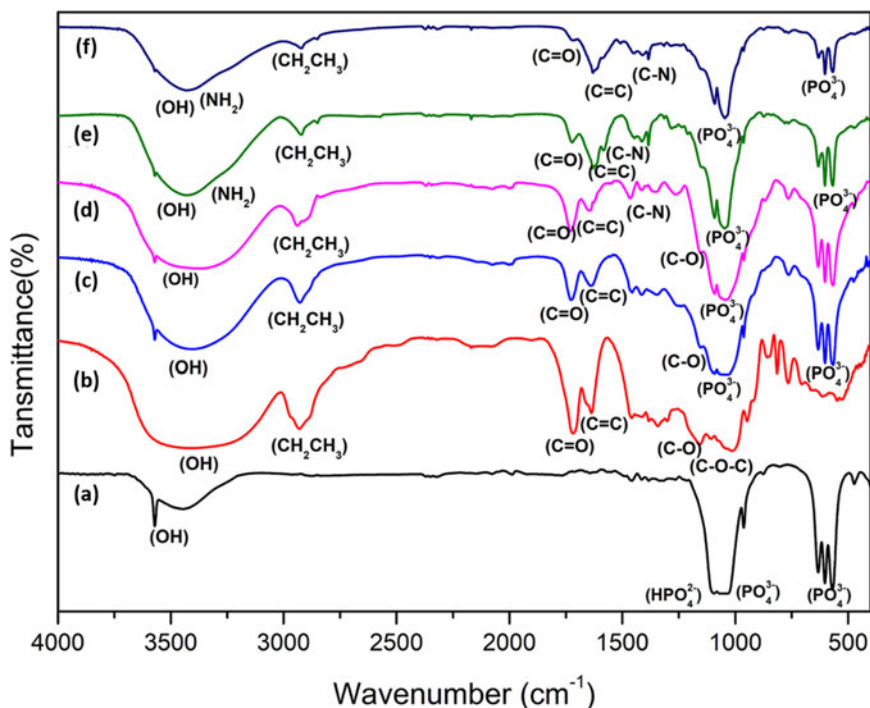


Figure 1: FTIR spectra of HA NPs (a), DEX-MA (b), DM-g-HA NPs (c), ODM-g-HA NPs(d), DOX-ODM-g-HA NPs (e) and MTX-DOX-ODM-g-HA NPs (f).

observed at 265.2 (84.52%) due to MTX and DOX loss and 340.01 (73.62%) to 505.01 (68.97%) due to polymer degradation [Fig. S1(e)].

The loss of polymer weight in the samples on heating indirectly resembles the polymer graft content of the NPs. From the TGA data, it is estimated that approximately 35–45% of polymer was grafted onto the NPs. The percentage polymer grafting onto the NPs determined by the weight percentage analysis showed $53.67 \pm 4.69\%$ (Table 1) and by the HA dissolution method showed $44.93 \pm 10\%$ (DM-g-HA NPs) and $54.16 \pm 3.8\%$ (ODM-g-HA NPs) (Table 2).

The mean particle size distribution of HA NPs, ODM-g-HA NPs, DOX-ODM-g-HA NPs and MTX-DOX-ODM-g-HA NPs was determined by dynamic light scattering and the results are tabulated in Table SI. The surface morphology and polymer grafting onto the NPs were also analyzed by TEM (Fig. 3). The synthesized NPs were irregular in shape and most of the particles were a combination of rod and spherical shapes. The NPs as prepared showed some agglomeration and it was relatively more for drug-loaded NPs. This may be due to some attraction (Electrostatic/Van der Waals) between the drugs in the drug-loaded NPs [36]. Other factors, such as wide particle size distribution and high particulate density of NPs, may contribute to agglomeration. TEM images (Fig. 3) clearly demonstrated that the synthesized NPs were core shell in structure with the diffused layer of polymeric DEX-MA graft as shell and dark ceramic HA as inner core. The DOX conjugation on the NPs does not show any difference in the

surface of the NPs meanwhile there is a change in the surface morphology of MTX-DOX-ODM-g-HA NPs which may be due to the physically adsorbed MTX [Fig. 3(d)].

Estimation of Drug Content

The amount of DOX conjugated onto the ODM-g-HA NPs was found to be $85.81 \pm 2.07\%$. The amount of MTX physically loaded onto the DOX-ODM-g-HA NPs was $87.31 \pm 4.37\%$. The MTX was also loaded onto the ODM-g-HA NPs and encapsulation efficacy was found to be $80.28 \pm 8.73\%$. The DOX conjugation efficacy was around 85% and it is indeed high compared to our previous work, where only 20% of MTX was conjugated onto the PVA-grafted HA NPs [31]. In the present work, dextran has been grafted onto the HA NPs and the large amounts of aldehyde groups generated in oxidized dextran facilitate the coupling of the amine groups in DOX via Schiff base resulting in more coupling efficacy. MTX loading on ODM-g-HA NPs and DOX-ODM-g-HA NPs did not show any significant changes in loading percentage. The amount of drug present in the final formulation (MTX-DOX-ODM-g-HA NPs) was 0.174 mg of MTX and 0.088 mg of DOX per mg of the NPs.

In vitro Drug Release

In vitro drug release studies were performed for MTX-DOX-ODM-g-HA NPs in acidic (PBS pH 5) and alkaline

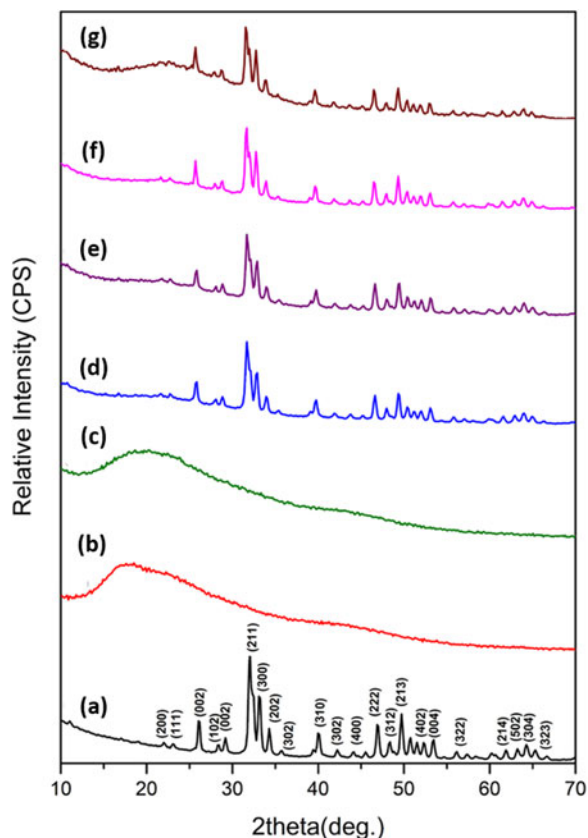


Figure 2: XRD spectra of HA NPs (a), Dextran (b), DEX-MA (c), DM-g-HA NPs (d), ODM-g-HA NPs (e), DOX-ODM-g-HA NPs (f) and MTX-DOX-ODM-g-HA NPs (g).

(PBS pH 7.4) environment for 10 days (Fig. 4). The maximum MTX release was $90.57 \pm 1.84\%$ (pH 5) and $78.53 \pm 7.4\%$ (pH 7.4). In case of DOX, the maximum release was $31.30 \pm 5.91\%$ (pH 5) and $11.50 \pm 1\%$ (pH 7.4). The drug release profile for DOX-ODM-g-HA NPs was also performed in pH 5 and pH 7.4 that showed a maximum release of $31.30 \pm 5.91\%$ and $13.55 \pm 0.85\%$, respectively [Fig. S2(a)]. The MTX loaded onto the ODM-g-HA NPs showed a release of $67.75 \pm 10.67\%$ (pH 5) and $57.12 \pm 8.29\%$ (pH 7.4) [Fig. S2(b)].

At acidic pH 5, MTX and DOX showed a higher drug release compared to the release profile in the slightly alkaline pH 7.4. This is attributed to the enhanced solubility of DOX and MTX in acidic condition. MTX showed initial burst release around 35–45% in both acidic and alkaline condition within 1 h. But in case of DOX, the release profile was pH dependent,

TABLE 1: Grafting efficiency by weight percentage analysis.

Batch	Initial weight of KPS HA NPs: DEX-MA (mg)	Final weight after grafting and lyophilization (mg)	Grafting efficiency (%)
1	200:200	317.4	58.7
2		301.4	52.9
3		298.8	49.4

TABLE 2: Grafting efficiency by dissolution method.

Sample name	Initial weight of polymer-grafted HA NPs (mg)	Final weight after dissolution and lyophilization (mg)	Grafting efficiency (%)
DM-g-HA NPs	50	22.46 ± 5	44.93 ± 10
ODM-g-HA NPs	50	21.23 ± 8.3	54.9 ± 4

at pH 7.4, only 12% was released meanwhile 20% burst release was observed at pH 5. This clearly indicates that covalently bound DOX (imine) is stable at normal physiological pH 7.4 but in acidic milieu (pH 5), imine linkage is more labile which leads to enhanced DOX release [37]. Around 75% of MTX (pH 5) was released within 48 h followed by sustained release of a maximum 90% at the end of 10 days. In case of DOX (pH 5), 35% was released at 48 h followed by a sustained release and maximum released was around 50%.

At physiological pH 7.4, within 24 h, around 65% of MTX was released and 78% was the maximum released at the end of 10 days. DOX at pH 7.4 does not show any burst release throughout the time period and the maximum release was around 12%. In our earlier report [31], physically adsorbed gemcitabine in the PVA-grafted HA NPs showed a maximum release of 60% at the end of 10 days at pH 7.4. But in the present case, the physical loading of MTX onto the ODM-g-HA NPs showed a 60% release within 24 h. Desorption/release of drug molecules depends upon the polymer matrix and polysaccharide-based hydrogels will absorb water leading to swelling of the matrix which increases the pore size resulting in enhanced drug release as shown by Miao et al. [38]. In this study, we have used ODM which behaves like a hydrogel resulting in higher drug release. To confirm this phenomenon, we performed swelling behavior of ODM-g-HA NPs, DM-g-HA NPs, HA NP and the results are shown in Fig. S3.

Swelling Studies

The amount of water absorbed onto the HA NPs and the polymer-grafted NPs were determined by swelling studies. It was seen that equilibrium swelling was achieved by all NPs in about 2 h (Fig. S3). The HA NPs showed an equilibrium swelling of $65.52 \pm 1.23\%$ whereas the DM-g-HA NPs and ODM-g-HA NPs showed equilibrium swelling of $71.42 \pm 1\%$ and $85.29 \pm 5.76\%$, respectively. From the results, it is evident that higher release percentages of physically loaded drug from the NPs are due to water absorption and swelling of ODM.

Drug Release Kinetics

In vitro drug dissolution studies have been documented as important parameters in drug formulation and development. Various theoretical/ kinetic models were developed to define the drug

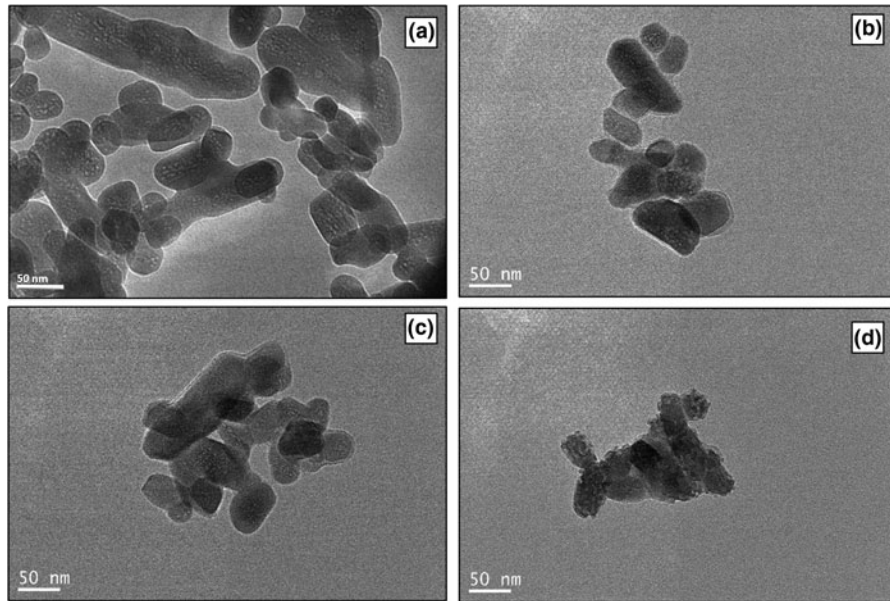


Figure 3: TEM images of HA NPs (a), ODM-g-HA NPs (b), DOX-ODM-g-HA NPs (c) and MTX-DOX-ODM-g-HA NPs (d).

release mechanisms from different formulations (immediate/controlled/sustained). A wide range of mathematical models were established to fit the drug dissolution data and most of them were nonlinear equations [39]. To understand the drug release mechanism from the nanocarrier, different models, such

as zero order, first order, Higuchi, Korsmeyer Peppas, Hixson Crowell, Hopfenberg and Weibull, were fitted with the drug release data. The mechanism of release was analyzed using the correlation coefficient (R^2) with other parameters and the values are tabulated and shown in Table SII. Among the different models, Korsmeyer Peppas and Weibull showed the highest R^2 values (0.96–0.98) for MTX-DOX-ODM-g-HA NPs in both PBS pH 7.4, as well as pH 5 buffers. Peppas model is a simple and semi empirical relationship which describes the drug release mechanism from the polymeric and matrix systems.

The equation of Korsmeyer–Peppas is

$$F = k_{KP} * t^n,$$

where F is the fraction of drug dissolved at time t , k_{KP} is the release constant including structural and geometric characteristics of the drug-dosage form and n is the diffusional release exponent. The “ n ” value specifies the release mechanism of drug molecules based on solvent diffusion rate (R_{diff}) and polymer chain relaxation rate (R_{relax}). For planar or cylindrical geometry, the value of $0.5 \leq n$ corresponds to Fickian diffusion in which the rate of solvent penetration was much smaller than the rate of polymer chain relaxation and the system controlled by diffusion ($R_{diff} \ll R_{relax}$), $0.5 < n < 0.89$ with non-Fickian transport mechanism where the diffusion and polymeric chain relaxation rates were comparable to each other ($R_{diff} \approx R_{relax}$), $n = 0.89$ with Case II transport, and $n > 0.89$ with super case II transport by zero order (swelling and controlled drug release) which defines the diffusion process was much faster than the relaxation process and the system controlled by relaxation ($R_{diff} \gg R_{relax}$). Sometimes, the solvent diffusion rate was

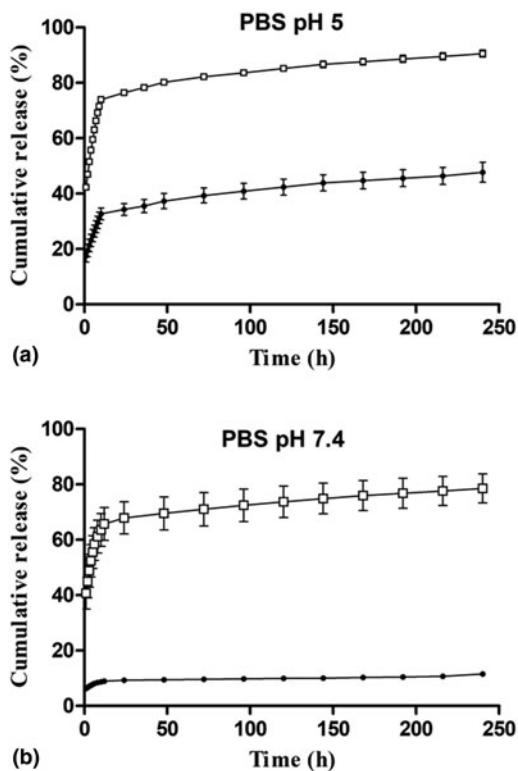


Figure 4: *In vitro* drug release profile of DOX (●) and MTX (□) from MTX-DOX-ODM-g-HA NPs at pH 5 (a) and pH 7.4 (b).

much below the relaxation rate, where the n value can be detected less than 0.5. This condition was also considered as Fickian diffusion, especially called as “Less Fickian” behavior [40]. In both acidic and alkali conditions, drug release profiles of MTX and DOX from the MTX-DOX-ODM-g-HA NPs showed n value of less than 0.5 which confirmed the mechanism behind the release of DOX and MTX from the nanocarrier was Fickian diffusion. Peppas model fit drug release curve of MTX and DOX from NPs at pH 7.4 and pH 5 are shown in Fig. S4.

Weibull is an empirical model and widely applied for extended release dosage forms, as well as matrix systems [41]. It can be used for all types of dosage forms and for drug release mechanisms, such as diffusion, dissolution and dissolution-diffusion rate. The equation of Weibull is

$$F = 100 * \{1 - e^{-(t/\alpha)^\beta}\}.$$

In this equation, F is the fraction of drug dissolved as a function of time t , α defines a scale parameter of geometry, β defines a shape parameter which explains about drug dissolution curve. In case $\beta = 1$, the shape of the curve corresponds to exponential, $\beta > 1$ defines the sigmoid S-shaped upward curve and if $\beta < 1$ denotes a parabolic with initial high slope followed by the consistent exponential.

Weibull model fit release curves of MTX and DOX are shown in Fig. S5. Overall, all the release profiles of MTX and DOX from MTX-DOX-ODM-g-HA NPs in both acidic and alkali conditions, β value was found to be less than 1 which denotes parabolic curve with high initial slope (Fig. S5). At pH 7.4, MTX release from MTX-DOX-ODM-g-HA NPs showed high β value (0.178) compared to the DOX (0.092) which shows the conjugated DOX from the ODM releases the drug in slow fashion compared to the physically loaded drug MTX. But in case of pH 5, no significant difference was observed in both MTX ($\beta = 0.202$) and DOX ($\beta = 0.252$), the release of drug molecules from the nanocarriers being dependent on acidic environment which may be the reason for higher drug release (similar β values). Scale parameter (α) defines the release rate of dissolved drug molecules, if scale parameter is high, drug release rate will be slower. Interestingly, DOX showed higher α values ($\alpha = 14.371$) at alkali environment (pH 7.4) compared to acidic condition pH 5 ($\alpha = 4.723$). Thus, the release of DOX from the nanocarrier showed a steady and sustained pattern. Meanwhile, physically loaded drug MTX showed α values of 1.706 (pH 7.4) and 1.626 (pH 5), which represent desorption of drug molecules through polymeric matrix leading to immediate release (Fig. S3). From the kinetic data, it is evident that conjugated drug (DOX) release from the nanocarrier mainly depends on the physiological environment, i.e., acidic (higher release) and alkali (slower release). In case of physically loaded drug (MTX) release from nanocarrier was

mainly based on the dissolution – diffusion from the polymeric matrix which followed the Fickian diffusion mechanism.

Biocompatibility Assay

Biocompatibility of implant materials is an essential requirement in bone tissue engineering. The biocompatibility of the NPs was evaluated according to ISO 10993 using L929 fibroblast cells [42]. The HA NPs, DM-g-HA NPs and ODM-g-HA NPs showed more than 80% cell viability at three different concentrations such as 0.25 mg, 0.5 mg and 1 mg/mL and hence were considered biocompatible (Fig. S6).

Cell Viability Studies

Indirect contact assay method was performed for testing the cytotoxicity of NPs and drug-loaded NPs. The NPs (0.5 to 5 mg/mL) were incubated in MEM media for 7 days and extracts were collected using 0.2 μ m syringe filter. Extracts from NPs were added to OMG 63 cells and incubated for 24 and 72 h. HA NPs, DM-g-HA NPs and ODM-g-HA NPs showed more than 80% viability at 24 h and more than 60% viability at 72 h incubation and there was no significant difference observed compared to control cells. At 24 h, drug-loaded samples, such as MTX-DOX-ODM-g-HA NPs, MTX-ODM-g-HA NPs and DOX-ODM-g-HA NPs, showed less than 60% viability at 5 mg/mL concentration whereas at 72 h, all the drug-loaded samples showed less than 50% cell viability and significant difference was observed between the HA NPs and drug-loaded NPs (Fig. 5).

The synergistic, additive or antagonistic effect of the multidrug-loaded NPs activity was calculated by combination index (CI) using Chou–Talaly method [43] as reported by Song et al. [44].

The equation for calculating CI index is

$$CI_x = \frac{(D)_1}{(D_x)_1} + \frac{(D)_2}{(D_x)_2},$$

where $(D_x)_1$ is inhibitory concentration (IC_x) value of drug 1, $(D_x)_2$ is inhibitory concentration (IC_x) value of drug 2. $(D)_1$ and $(D)_2$ are concentrations of drug 1 and drug 2 in the combined systems at particular IC_x value. The CI values represent the synergistic, additive or antagonist effect ($CI < 1$ synergistic effect, $CI = 1$ additive effect and $CI > 1$ antagonist effect). CI values for 24 and 72 h incubated samples were calculated and are shown in Table 3. The combination effect was calculated using CI plot at 72 h incubation (Fig. S7).

Dual drug-loaded MTX-DOX-ODM-g-HA NPs showed synergistic activity compared to the single drug-loaded NPs and the synergistic activity was calculated by CI using Chou–Talaly equation. Additive effect was observed at 24 h incubation and CI_{25} and CI_{50} showed values equal to 1 (Table 3).

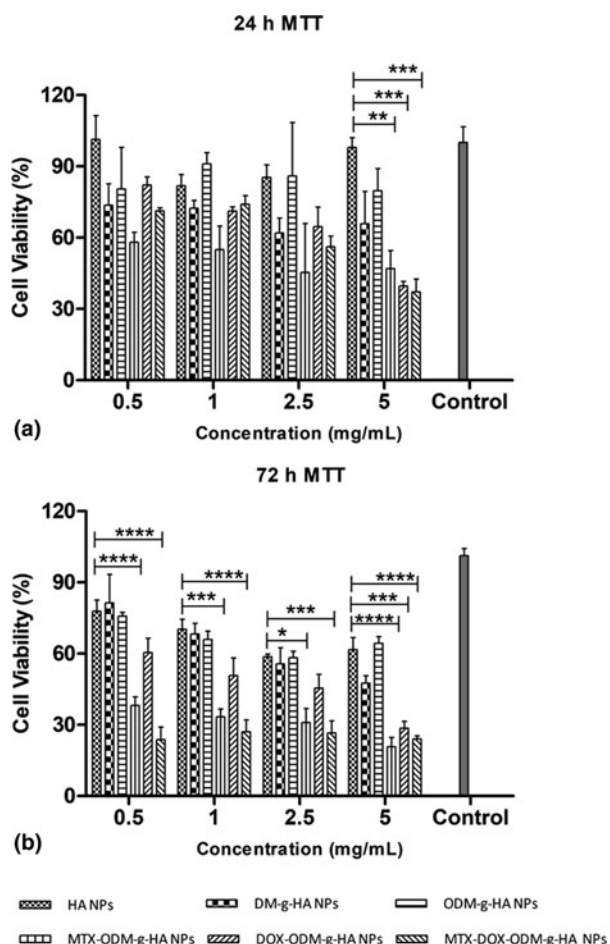


Figure 5: Cytotoxicity assay on OMG 63 cells for HA NPs, DM-g-HA NPs, ODM-g-HA NPs, MTX-ODM-g-HA NPs, DOX-ODM-g-HA NPs and MTX-DOX-ODM-g-HA NPs at 24 and 72 h incubation.

In case of 72 h incubation, the CI values were less than 1 for CI_{50} and CI_{75} . The CI_x values plotted with respect to drug effect is shown in Fig. S7. The cell viability assay and CI plot index conclusively established the synergistic effect of MTX and DOX. These results are in agreement with previous work reported by Ma et al. [9] and Rahimi et al. [45].

Cellular Uptake Studies

The intracellular uptake of RhB labeled HA NPs, ODM-g-HA NPs, DOX-ODM-g-HA NPs and MTX-DOX-ODM-g-HA

TABLE 3: CI_x values of MTX-DOX-ODM-g-HA NPs at 24 and 72 h incubation in OMG-63 cells.

Time point (h)	MTX-DOX-ODM-g-HA NPs			
	CI_x	CI_{MTX}	CI_{GEM}	CI_{Total}
24	CI_{25}	1	0.2	1
	CI_{50}	0.5	0.5	1
72	CI_{50}	0.5	0.2	0.7
	CI_{75}	0.2	0.1	0.3

NPs was tested using the OMG 63 cells. Nucleus was stained with Hoechst (blue fluorescence), cytoplasm was stained with FDA (green fluorescence) and RhB labeled NPs gave red fluorescence. Uptake and localization of the NPs were observed under confocal microscope at 10× magnification as shown in Fig. 6. The uptake was confirmed by the appearance of red fluorescence compared to the control samples. It is clearly seen that NPs are localized only in the cytoskeleton and around the nucleus at 24 h incubation (Fig. 6).

The internalization of RhB labeled NPs was also quantified by flow cytometry and results are shown in Fig. S8. At 24 h incubation, uptake was more than 90% for all the samples (Fig. S8). Drug-loaded samples showed higher fluorescence intensity compared to other samples. The mean fluorescence intensity of HA NPs, DM-g-HA NPs and ODM-g-HA NPs was found to be 2693.5 ± 296.27 , 2460.5 ± 135.05 , 3755.5 ± 450.43 and for DOX-ODM-g-HA NPs and MTX-DOX-ODM-g-HA NPs was $12,946.5 \pm 115.25$ and 5219 ± 45.25 , respectively. Significant difference was noted and there was a right shift in DOX-ODM-g-HA NPs and MTX-DOX-ODM-g-HA NPs compared to control and other samples (HA NPs, DM-g-HA NPs and ODM-g-HA NPs) (Fig. S8). DOX-ODM-g-HA NPs showed higher fluorescence intensity compared to the other samples, such as HA NPs, DM-g-HA NPs, ODM-g-HA NPs and MTX-DOX-ODM-g-HA NPs, which may be due to the combined fluorescence effect of DOX and rhodamine on the NPs.

Gene Expression Studies

The gene expression levels of BAX and Caspase 3 in DOX-g-HA NPs, MTX-DOX-g-HA NPs and untreated samples were analyzed by quantitative real-time PCR. From the results, it is clearly seen that expression levels of BAX and caspase 3 in drug-loaded samples showed upregulation compared to the untreated samples (Fig. 7). Initial stages of apoptosis are described by morphological parameters like cell shrinkage, chromatin condensation, membrane blebbing and nuclear fragmentation. Apoptosis is based on the gene regulation and it is imperative to understand the mechanism of cell proliferation, differentiation and tumor biology [46]. Numerous diseases and disorders are due to the defects in apoptotic pathways [46]. Chemotherapy leads to the regulation of apoptotic genes like BAX and caspase family to induce the apoptosis of osteosarcoma cells [9]. Using quantitative RT-PCR, apoptosis-associated gene expression levels of drug-loaded NPs were evaluated (Fig. 7). Caspase-3 and BAX were exposed to the NPs treated MG63 cells. Compared to the untreated group, drug-loaded NPs treated cells showed higher expression levels. Interestingly, dual drug-loaded MTX-DOX-ODM-g-HA NPs showed enhanced expression of BAX and caspase-3

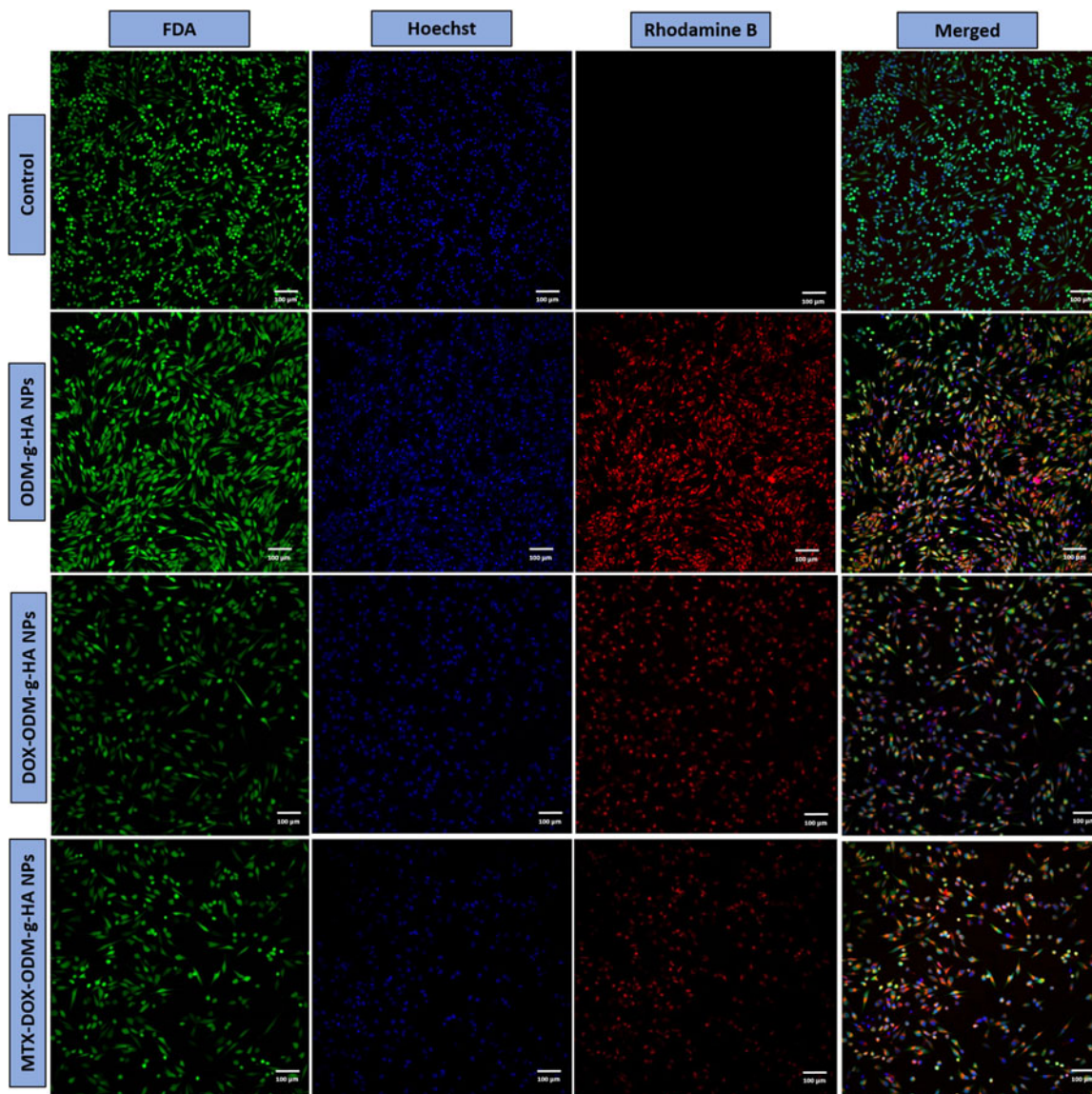


Figure 6: Cell uptake of HA NPs, ODM-g-HA NPs, DOX-ODM-g-HA NPs and MTX-DOX-ODM-g-HA NPs in OMG 63 cells by confocal microscopy.

compared to the untreated, as well as DOX-g-ODM-HA NPs (Fig. 7).

Hemocompatibility

Hemolysis assay was performed to determine the hemocompatibility and to examine the effect of different NPs on membrane integrity of human red blood cells (RBCs). All the tested samples at concentrations ranging from 0.5 to 2.5 mg/mL of NPs showed less than 2% hemolysis (Fig. S9) confirming their non-toxicity and compatibility with RBCs. Moreover, HA NPs, DM-g-HA NPs and ODM-g-HA NPs showed less than 0.5–1% hemolysis from lower to higher concentration (Fig. S9) clearly demonstrating that the NPs systems were highly hemocompatible. The membrane integrity and morphology of the RBCs treated with

the NPs were examined using optical microscopy. RBCs treated with water showed hemolysis of more than 80%. The images of the untreated RBCs (in PBS) were compared with the NPs treated with RBCs and are shown in Fig. S10. After treatment with the NPs, images of the RBCs confirmed that there was no significant difference between the control samples and treated ones whereas RBCs treated with water showed lysis (Fig. S10). All the samples were highly hemocompatible and did not show any significant difference between untreated and NPs treated samples.

Conclusions

In this study, MTX and DOX-loaded HA NPs with a ceramic core and dextran shell were fabricated and investigated as a

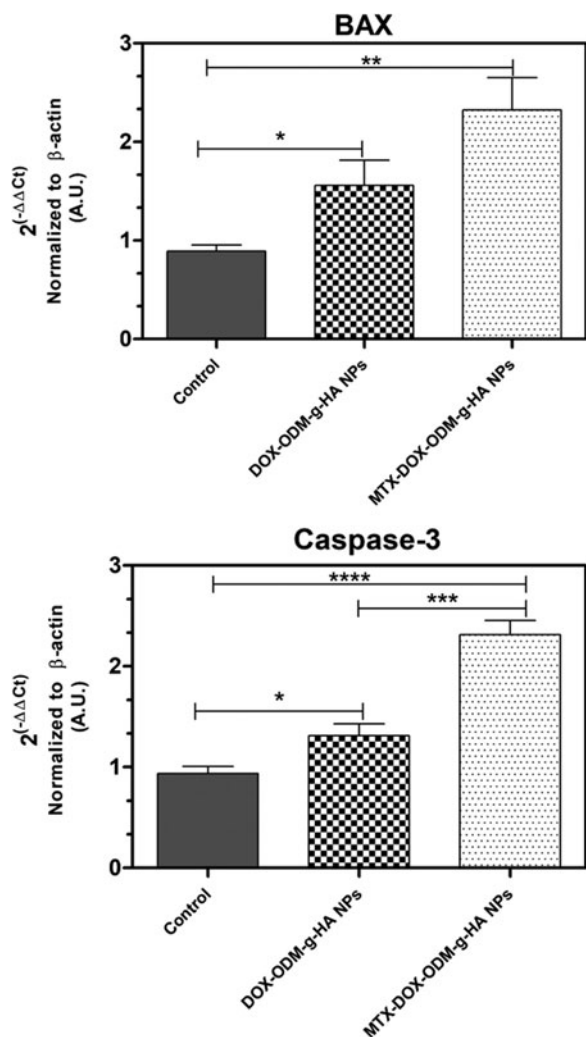


Figure 7: Effect of DOX and MTX-DOX loaded ODM-g-HA NPs on the expression of apoptotic genes in OMG 63 cells at 24 h incubation. The concentration of NPs was 1 mg/mL. Apoptotic genes caspase-3 and BAX were analyzed and β -actin was included as a house keeping gene. Data were normalized to β -actin ($n = 3$).

bone filling material for combinatorial delivery of drugs for the treatment of bone cancer. Dextran methacrylate was grafted onto the HA NPs with a grafting efficiency of 40–50%. Oxidation of grafted dextran using periodate generated aldehyde functions on the polysaccharide which was used to couple DOX through Schiff base formation with a coupling efficacy of 85%. MTX was physically loaded onto the DOX-conjugated NPs thereby enabling the delivery of two drugs from the NPs at different rates. The core-shell architecture of the NPs was confirmed by TEM. *In vitro* drug release studies showed sequential release of MTX followed by DOX for more than week in a sustained manner. These dual drug-loaded NPs showed a synergistic effect in *in vitro* cytotoxicity studies, as well as in gene expression studies. Further, the effect on apoptosis by the combination of MTX and DOX was confirmed

by increased regulation of apoptotic-related genes of caspase-3 and BAX. The NPs were non-toxic and showed good biocompatibility and hemocompatibility. These NPs are expected to be effective as bone void filling material and for synergistic therapy for the treatment of bone cancer.

Materials and Methods

Synthesis of dextran methacrylate

The synthesis of dextran methacrylate was carried out according to a procedure of Kim and Chu [47]. Briefly, 1 g of dextran was accurately weighed and dissolved in 10 mL DMF containing 10% lithium chloride at 90 °C under nitrogen atmosphere in a round-bottomed flask of 50 mL capacity. The mixture was cooled and maintained at 60 °C. Triethylamine (equivalent to 1 mol% of methacrylic anhydride) was then added and magnetically stirred for 15 min. Then, methacrylic anhydride (1 mol%) was slowly added to the mixture and stirred for 10 h at 60 °C, cooled to room temperature and precipitated using cold isopropyl alcohol (IPA). The product was washed several times with IPA and dried in a vacuum oven at room temperature. The product was named as DEX-MA.

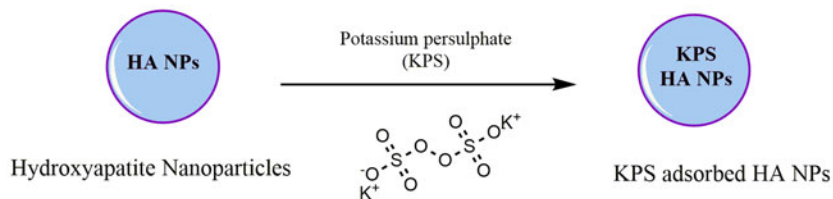
Synthesis of HA NPs

HA NPs were synthesized by wet chemical precipitation technique using a modified procedure of Zhang and Lu [48]. The precursors, such as calcium nitrate (0.5 M) and diammonium hydrogen phosphate (0.5 M), were quickly mixed using a magnetic stirrer. Calcium and phosphate molar ratio was maintained at 1.67. The reaction was carried out at 40 °C for 4 h in a constant temperature bath while the pH was maintained at 10.5 to 11. The reaction mixture was incubated in an air oven at 40 °C for overnight and the product was centrifuged at 12,000 rpm for 30 min. The pellets were washed with water several times to remove the impurities. Then the samples were dried in a hot air oven at 100 °C overnight and further heated at 800 °C in a muffle furnace for 1 h. The product yield was around 60–70%.

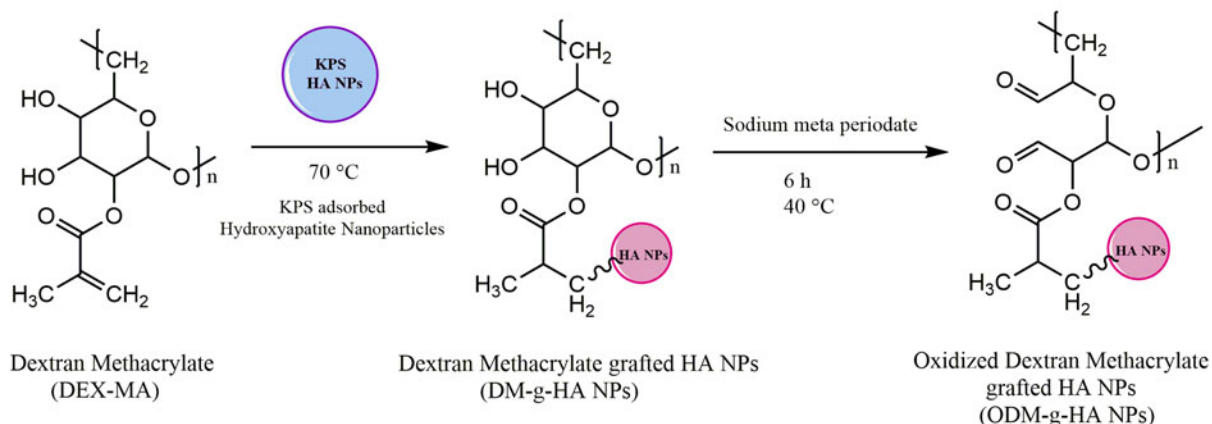
DEX-MA grafting on HA NPs

Into 10 mL of a 1% solution of potassium persulphate (KPS), 200 mg of HA NPs were added and incubated for 24 h at room temperature. After incubation, the mixture was centrifuged at 10,000 rpm and pellets were separated and dried in a vacuum desiccator. The DEX-MA polymer was grafted onto the HA NPs by emulsion polymerization technique. The schematic representation of grafting DEX-MA onto HA NPs is shown in Scheme 1 (Step 2).

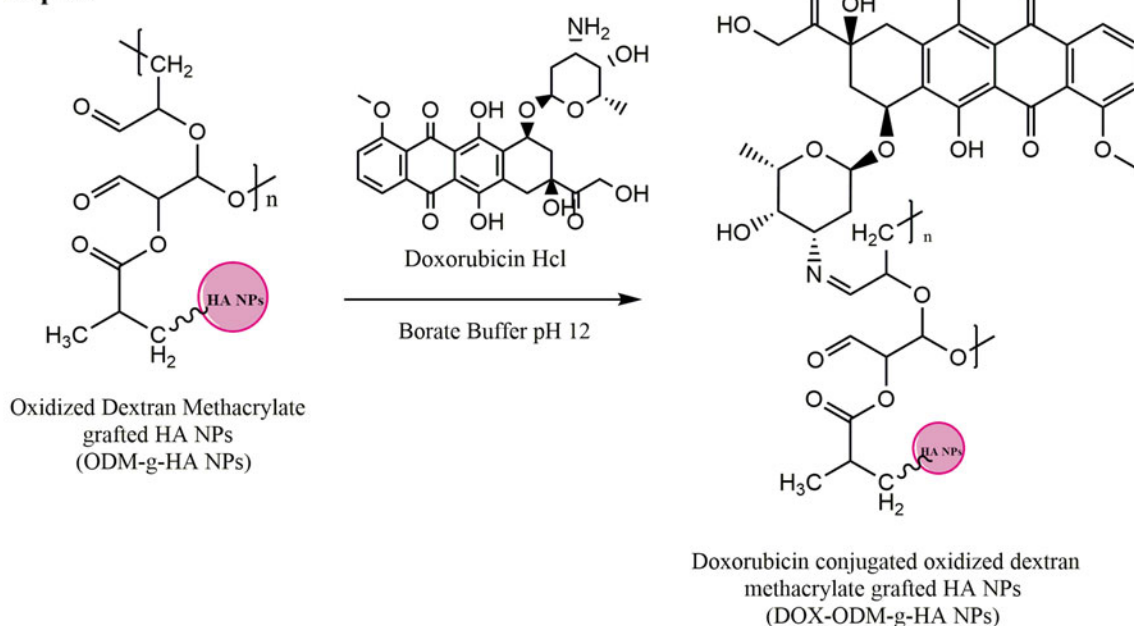
Step : 1



Step : 2



Step : 3



Scheme 1: Synthesis of doxorubicin-conjugated ODM-grafted HA NPs (DOX-ODM-g-HA NPs).

Briefly, 200 mg of DEX-MA was dissolved in 20 mL water in a 50 mL pressure tube and KPS-treated HA NPs (200 mg) was added into the solution. After purging the reaction mixture

with argon for 2 h, the tube was heated in an oil bath under magnetic stirring at 70 °C for 24 h. The contents were cooled to room temperature and centrifuged at 12,000 rpm for

30 min. The sedimented NPs were washed with water (3×) to remove the unreacted monomer. The product was lyophilized and stored at room temperature. DEX-MA-grafted HA NPs are named as DM-g-HA NPs.

Oxidation of DM-g-HA NPs

The oxidation was carried out using sodium meta periodate. Into 100 mg of DM-g-HA NPs dispersed in 10 mL water, 0.2 equivalence of periodate was added to achieve 20% oxidation. The reaction was carried out in dark at 40 °C for 6 h under magnetic stirring. The reaction was stopped by the addition of a few drops of ethylene glycol, and the contents were dialyzed against water for 48 h with several changes of water, frozen, lyophilized and stored at room temperature. The procedure is shown in Scheme 1 (Step 2). The oxidized DM-g-HA NPs are designated as ODM-g-HA NPs.

Estimation of graft content

The graft percentages were calculated by two methods. (i) From the change in weight of the HA NPs using the following formula

$$\text{Graft (\%)} = \frac{\text{Final weight of NPs after reaction} - \text{Initial weight of HA NPs}}{\text{Initial weight of HA NPs}} \times 100$$

and (ii) by dissolving the NPs in 1 M HCl as reported in our previous work [31]. Into 10 mL of 1 M HCl, 50 mg of DM-g-HA NPs or ODM-g-HA NPs was added and stirred for 5 min at room temperature to completely dissolve the HA. The contents were then centrifuged and the supernatant was removed. The pellets were washed with water and dried. The amount of grafting was calculated by the following equation

$$\text{Graft (\%)} = \frac{\text{Weight of the NPs after dissolution of the HA}}{\text{Initial weight of polymer grafted HA NPs}} \times 100.$$

DOX conjugation onto ODM-g-HA NPs

DOX was conjugated onto ODM-g-HA NPs by Schiff base reaction. The ODM-g-HA NPs (100 mg) were dispersed in 10 mL borate buffer of pH 12. DOX (10 mg) was added to the solution and mixture was stirred magnetically at 40 °C in dark for 24 h. The content was centrifuged and the supernatant was separated and the precipitate was dialyzed against water for 48 h using the dialysis bag of MWCO 6–8 kDa frozen, lyophilized and stored at 4 °C. The product is named as

DOX-ODM-g-HA NPs. The reaction protocol is shown in Scheme 1 (Step 3).

MTX loading onto DOX-ODM-g-HA NPs

MTX was loaded onto the NPs by the physical adsorption method. Briefly, 10 mg of MTX was dissolved in 2 mL borate buffer of pH 12 in a 10 mL round-bottomed flask and 50 mg of DOX-ODM-g-HA NPs or ODM-g-HA NPs was added. The reaction mixture was incubated at 4 °C (cold room) for 24 h. Then the contents were centrifuged, supernatant separated and pellets were lyophilized and stored at 4 °C. The resultant NPs are designated as MTX-DOX-ODM-g-HA NPs and MTX-ODM-g-HA NPs.

Estimation of drug content

The amounts of DOX conjugated and MTX loaded onto the NPs were calculated by the indirect estimation method. After 24 h incubation of NPs in 2 mL borate buffer, the NPs were centrifuged and the supernatant was diluted using borate buffer of pH 12 and the drug contents were estimated using UV–Visible spectroscopy at 481 nm (DOX) and 302 nm (MTX). The DOX conjugation efficiency and MTX loading efficiency were calculated by using a calibration curve of DOX and MTX in borate buffer at pH 12.

$$\text{Percentage of drug loaded} = \frac{\text{Final concentration of drug in the supernatant}}{\text{Initial concentration of drug added to NPs}} \times 100.$$

In vitro drug release

DOX-ODM-g-HA NPs, MTX-ODM-g-HA NPs and MTX-DOX-ODM-g-HA NPs (2 mg each) were weighed and transferred into 20 mL glass flat bottomed vials. Then 10 mL of PBS pH 7.4 and pH 5 were added into the vials and incubated in a constant temperature bath at 37 °C. Sink conditions were maintained during the release studies. Aliquots of 1 mL supernatant were withdrawn at different time points and replaced with fresh PBS. The amount of released drug in the media was estimated by measuring the absorbance of samples at 480 nm (DOX) and 302 nm (MTX) using UV–visible spectroscopy by employing calibration curves of the drugs in PBS of pH 7.4 and 5.

Swelling studies

HA NPs, DM-g-HA NPs and ODM-g-HA NPs (50 mg) were accurately weighed and transferred into pre-weighed falcon tubes. Then, 10 mL of PBS pH 7.4 was added and incubated

at room temperature for 6 h. Every 1 or 2 h, the samples were centrifuged, the supernatant was removed and the falcons were weighed till equilibrium swelling was achieved. The extent of swelling was calculated using the following formula,

$$\text{Swelling (\%)} = \frac{\text{Wt. of swollen NPs} - \text{Wt. of dry NPs}}{\text{Wt of swollen NPs}} \times 100.$$

Cell culture studies

Biocompatibility assay

The biocompatibility of HA NPs, DM-g-HA NPs and ODM-g-HA NPs was tested using L929 fibroblast cells by MTT assay. The cells were grown in DMEM with 10% FBS and 1% antibiotic–antimycotic solution at 37 °C with 5% carbon dioxide (CO₂) in an incubator. The cells were maintained by changing media at regular intervals until cells attained more than 80% confluence. The cells were seeded in 24-well plates with a seeding density of 1 × 10⁵ cells/well and incubated at 37 °C with 5% CO₂ for 24 h. Then, 0.25, 0.5 and 1 mg of HA NPs, DM-g-HA NPs and ODM-g-HA NPs were added to 1 mL of DMEM and the samples were sonicated for 15 min and 100 μL of NPs dispersed DMEM were added into the wells and incubated for 24 h. After incubation, the DMEM was replaced with 90 μL of DMEM and 10 μL of MTT (5 mg/mL stock) and the cells were incubated for 4 h at 37 °C for the formation of formazan crystals. The supernatant was removed and DMSO was added to each well to solubilize the formazan crystals and the absorbance at 570 nm was measured using a microplate reader. The cell viability was calculated from the ratio of sample absorbance and control absorbance.

Cytotoxicity assay

Cytotoxicity assay was performed using MTT by indirect contact method with OMG 63 cells. Briefly, 0.5, 1, 2.5 and 5 mg of each HA NPs, DM-g-HA NPs, ODM-g-HA NPs, DOX-ODM-g-HA NPs, MTX-ODM-g-HA NPs and MTX-DOX-ODM-g-HA NPs was added to 1 mL MEM and kept in an orbital shaker maintained at 150 rpm at 37 °C for 7 days. The samples were centrifuged and filtered using a 0.2 μm Acrodisc sterile syringe filter (PALL Corporation, Port Washington, New York, USA). The extracted samples were stored at 4 °C and used for MTT assay. OMG 63 cells were seeded in 96-well plates with a density of 5000 cells/well. The extract (100 μL) was added to each well and incubated at 37 °C with 5% CO₂ for 24 and 72 h. The MTT assay was performed by the procedure as mentioned in the section "Biocompatibility assay".

Cell uptake studies

Rhodamine B (RhB) (1 mg/mL) stock was prepared in water and 1 mg each of ODM-g-HA NPs, DOX-ODM-g-HA NPs and MTX-DOX-ODM-g-HA NPs was added and the samples were kept in a bath sonicator for 30 min. Then the samples were spun at 50 rpm for 24 h using Rotospin. After incubation, the samples were centrifuged at 12,000 rpm for 15 min and pellets were dispersed in 1 mL of MEM and sonicated for 30 min.

OMG 63 cells were seeded in six-well plates with a seeding density of 1 × 10⁶ cells and the plates were incubated for 24 h at 37 °C with 5% CO₂. The RhB-loaded NPs (1 mg/mL) were added to the wells and incubated at 37 °C for 24 h in dark. After incubation, the media was removed and cells were washed with PBS repeatedly. The cells were incubated with Hoechst 33342 and FDA to stain the nucleus and cytoskeleton and subsequently washed repeatedly with PBS to remove the excess dyes and imaged using a laser confocal microscope (Olympus FV 3000, Japan).

Flow cytometry

HA NPs, ODM-g-HA NPs, DOX-ODM-g-HA NPs and MTX-DOX-ODM-g-HA NPs were tagged with RhB as described in the section "Cell uptake studies". The OMG 63 cells were seeded in six-well plates with a density of 2 × 10⁶ cells per well and incubated at 37 °C/ 5% CO₂ for 24 h. The RhB tagged samples (1 mg/mL) were added to the cells and incubated for 24 h. After incubation, the samples were washed with PBS and trypsinized to detach the cells, centrifuged at 1500 rpm for 5 min and cell pellets were collected. The pellets were suspended in PBS (300 μL) and the uptake of the NPs in the cells was determined by using flow cytometry (BD FACSVerser™, BD Biosciences, San Jose, CA, USA).

Gene expression studies

The protocol for conducting the gene expression studies was adopted from Ma et al. [9]. Using real-time PCR, the apoptosis-related gene (Caspase 3 and BAX) expression was determined by incubating the drug-loaded NPs in OMG 63 cells. Cells were seeded in 12-well plates with a density of 1 × 10⁶ cells per well and incubated at 37 °C for 24 h using a media composition of MEM with 10% FBS and 1% antibiotic–antimycotic solution. DOX-ODM-g-HA NPs and MTX-DOX-ODM-g-HA NPs (1 mg/mL) were incubated in MEM media for 7 days in the bath incubator shaker at 150 rpm at 37 °C for extraction. After incubation, the samples were filtered using 0.2 μm syringe filter.

The filtered media were added to the OMG cells in the 12-well plate and incubated for 24 h. Using TRIzol reagent, the total RNA was isolated from the OMG 63 cells.

Conversion of cDNA from the extracted RNA was done using a reverse transcription kit (Takara, Japan). Real-time PCR was performed by using Quant Studio Flex7 (Applied Biosystems, Waltham, Massachusetts, USA) with SYBR Premix Ex Taq kit (Takara, Japan). The specific primers such as Caspase 3 and BAX were used for apoptotic gene expression. β -actin was used as housekeeping gene and primer sequences used are shown in Table SIII. The transcript levels of the genes were normalized with respect to β -actin and the fold change was calculated by $2^{-\Delta\Delta Ct}$ method.

Hemocompatibility

The protocol for the hemolysis was adopted from a previous report by Francis et al. [49]. Briefly, whole human blood was collected from the blood bank using EDTA coated vacutainers. The RBCs were separated by centrifuging at 1500 rpm for 5 min. The supernatant plasma was removed and the sedimented RBCs were washed with saline (150 mM) thrice. After the final wash, the RBCs were dispersed in PBS (pH 7.4) and diluted to 10% of initial concentration.

Different concentrations of HA NPs, DM-g-HA NPs, ODM-g-HA NPs, DOX-ODM-g-HA NPs and MTX-DOX-ODM-g-HA NPs (0.5, 1, 2 and 2.5 mg) were used. The samples were sterilized by irradiation using UV radiation (254 nm, 30 W) for 2 h in a bio-safety cabinet and 200 μ L of suspended RBCs were added to all the samples and final volume was made up to 1 mL using PBS. The control samples were prepared without NPs. RBCs dispersed in water and PBS were used as positive and negative control, respectively. The samples were incubated at 37 °C for 1 h, centrifuged at 1500 rpm for 5 min and the absorbance of the supernatant was measured at 540 nm using a microplate reader. The percentage hemolysis was calculated by using the formula,

$$\text{Hemolysis (\%)} = \frac{\text{Absorbance of the sample} - \text{Absorbance of negative control}}{\text{Absorbance of positive control}} \times 100.$$

Evaluation of erythrocyte membrane integrity

Hemocompatibility is one of the imperative issues related to implanted biomaterials since RBCs will be lysed when in contact with the aqueous environment. Therefore, synthesized materials should preserve the erythrocyte integrity and functions in whole blood [50]. Membrane integrity was analyzed by optical microscopy. The NPs (1 mg/mL) were added to 200 μ L of suspended RBCs and incubated at 37 °C for 1 h in a constant temperature bath. The samples were centrifuged at 1500 rpm for 5 min and the RBC pellets were suspended in

500 μ L PBS of pH 7.4. The suspended RBC samples (10 μ L) were placed on glass slides and imaged using the optical microscope (Nikon Eclipse 2000i, Japan).

Acknowledgments

The authors thank Prof. Nitish R. Mahapatra for providing cell culture facility and thanks are due to Mr. Abrar Ali Khan and Mrs. Hemalatha who helped in gene expression studies. The authors thank Professor Sakthi Kumar of Toyo University, Japan for the TEM analysis. The authors also thank Central XRD Facility and Sophisticated Analytical Instrument Facility (SAIF) of IIT Madras for analytical support. This research did not receive any specific grant from any funding agencies in the public, commercial or not-for-profit sectors.

Supplementary material

To view supplementary material for this article, please visit <https://doi.org/10.1557/jmr.2020.193>

References

1. **T. Ibrahim, L. Mercatali, and D. Amadori:** Bone and cancer: The osteoncology. *Clin. Cases Miner. Bone Metab.* **10**, 121 (2013).
2. **J.T. Buijs and G. van der Pluijm:** Osteotropic cancers: From primary tumor to bone. *Cancer Lett.* **273**, 177–193 (2009).
3. **T. Kimura:** Multidisciplinary approach for bone metastasis: A review. *Cancers* **10**, 156 (2018).
4. **W. Gu, C. Wu, J. Chen, and Y. Xiao:** Nanotechnology in the targeted drug delivery for bone diseases and bone regeneration. *Int. J. Nanomedicine* **8**, 2305–2317 (2013).
5. **F. Macedo, K. Ladeira, F. Pinho, N. Saraiva, N. Bonito, L. Pinto, and F. Gonçalves:** Bone metastases: An overview. *Oncol. Rev.* **11**, 321 (2017).
6. **S. Hossen, M.K. Hossain, M.K. Basher, M.N. Mia, M.T. Rahman, and M.J. Uddin:** Smart nanocarrier-based drug delivery systems for cancer therapy and toxicity studies: A review. *J. Adv. Res.* **15**, 1–18 (2019).
7. **C. Marques, J.M. Ferreira, E. Andronescu, D. Fikai, M. Sonmez, and A. Fikai:** Multifunctional materials for bone cancer treatment. *Int. J. Nanomedicine* **9**, 2713–2725 (2014).
8. **E.M. Alexandrino, S. Ritz, F. Marsico, G. Baier, V. Mailänder, K. Landfester, and F.R. Wurm:** Paclitaxel-loaded polyphosphate nanoparticles: A potential strategy for bone cancer treatment. *J. Mater. Chem. B.* **2**, 1298 (2014).
9. **H. Ma, C. He, Y. Cheng, Z. Yang, J. Zang, J. Liu, and X. Chen:** Localized co-delivery of doxorubicin, cisplatin, and methotrexate by thermosensitive hydrogels for enhanced osteosarcoma treatment. *ACS Appl. Mater. Interfaces* **7**, 27040–27048 (2015).

10. **J.A. Kemp, M.S. Shim, C.Y. Heo, and Y.J. Kwon:** “Combo” nanomedicine: Co-delivery of multi-modal therapeutics for efficient, targeted, and safe cancer therapy. *Adv. Drug Deliv. Rev.* **98**, 3–18 (2016).
11. **P. Parhi, C. Mohanty, and S.K. Sahoo:** Nanotechnology-based combinational drug delivery: An emerging approach for cancer therapy. *Drug Discov. Today.* **17**, 1044–1052 (2012).
12. **A. Wicki, D. Witzigmann, V. Balasubramanian, and J. Huwyler:** Nanomedicine in cancer therapy: Challenges, opportunities, and clinical applications. *J. Control. Release* **28**, 138–157 (2015).
13. **C.M. Hu, S. Aryal, and L. Zhang:** Nanoparticle-assisted combination therapies for effective cancer treatment. *Ther. Deliv* **1**, 323–334 (2010).
14. **S.S. Qi, J.H. Sun, H.H. Yu, and S.Q. Yu:** Co-delivery nanoparticles of anti-cancer drugs for improving chemotherapy efficacy. *Drug Deliv.* **24**, 1909–1926 (2017).
15. **M. Estanqueiro, M.H. Amaral, J. Conceicao, and J.M. Lobo:** Nanotechnological carriers for cancer chemotherapy: The state of the art. *Colloids Surf. B: Biointerfaces* **126**, 631–648 (2015).
16. **C.Y. Zhao, R. Cheng, Z. Yang, and Z.M. Tian:** Nanotechnology for cancer therapy based on chemotherapy. *Molecules.* **23**, 826 (2018).
17. **M. Sadat-Shojai, M.T. Khorasani, E. Dinpanah-Khoshdargi, and A. Jamshidi:** Synthesis methods for nanosized hydroxyapatite with diverse structures. *Acta Biomater.* **9**, 7591–7621 (2013).
18. **X. Cheng and L. Kuhn:** Chemotherapy drug delivery from calcium phosphate nanoparticles. *Int. J. Nanomedicine* **2**, 667 (2007).
19. **L. Yang, B.W. Sheldon, and T.J. Webster:** Nanophase ceramics for improved drug delivery. *Am. Ceram. Soc. Bull.* **89**, 24–32 (2010).
20. **K.D. Son and Y.J. Kim:** Anticancer activity of drug-loaded calcium phosphate nanocomposites against human osteosarcoma. *Biomater. Res.* **21**, 13 (2017).
21. **W.M. Li, C.W. Su, Y.W. Chen, and S.Y. Chen:** In situ DOX-calcium phosphate mineralized CPT-amphiphilic gelatin nanoparticle for intracellular controlled sequential release of multiple drugs. *Acta Biomater.* **15**, 191–199 (2015).
22. **A. Lebugle, A. Rodrigues, P. Bonneville, J.J. Voigt, P. Canal, and F. Rodriguez:** Study of implantable calcium phosphate systems for the slow release of methotrexate. *Biomaterials.* **23**, 3517–3522 (2002).
23. **M.F. Cipreste and E.M.B. Sousa:** Poly(vinyl alcohol)/collagen/hydroxyapatite nanoparticles hybrid system containing yttrium-90 as a potential agent to treat osteosarcoma. *J. Biomater. Nanobiotechnol.* **5**, 24–30 (2014).
24. **Z.J. Rong, L.J. Yang, B.T. Cai, L.X. Zhu, Y.L. Cao, G.F. Wu, and Z.J. Zhang:** Porous nano-hydroxyapatite/collagen scaffold containing drug-loaded ADM-PLGA microspheres for bone cancer treatment. *J. Mater. Sci. Mater. Med.* **27**, 89 (2016).
25. **Y. Wang, X. Zhang, J. Yan, Y. Xiao, and M. Lang:** Surface modification of hydroxyapatite with poly(methyl methacrylate) via surface-initiated ATRP. *Appl. Surf. Sci.* **257**, 6233–6238 (2011).
26. **Q. Liu, J.R. de Wijn, and C.A. Van Blitterswijk:** Covalent bonding of PMMA, PBMA, and poly (HEMA) to hydroxyapatite particles. *J. Biomed. Mater. Res.* **40**, 257–263 (1998).
27. **Q. Liu, J.R. de Wijn, K. de Groot, and C.A. van Blitterswijk:** Surface modification of nano-apatite by grafting organic polymer. *Biomaterials* **19**, 1067–1072 (1998).
28. **S. Kango, S. Kalia, A. Celli, J. Njuguna, Y. Habibi, and R. Kumar:** Surface modification of inorganic nanoparticles for development of organic–inorganic nanocomposites – a review. *Prog. Polym. Sci.* **38**, 1232–1261 (2013).
29. **J. Wei, P. He, A. Liu, X. Chen, X. Wang, and X. Jing:** Surface modification of hydroxyapatite nanoparticles with thermal-responsive PNIPAM by ATRP. *Macromol. Biosci.* **9**, 1237–1246 (2009).
30. **A. Matsuda, T. Furuzono, D. Walsh, A. Kishida, and J. Tanaka:** Surface modification of a porous hydroxyapatite to promote bonded polymer coatings. *J. Mater. Sci. Mater* **14**, 973–978 (2003).
31. **S.R. Prasad, A. Jayakrishnan, and T.S. Sampath Kumar:** Hydroxyapatite-poly(vinyl alcohol) core-shell nanoparticles for dual delivery of methotrexate and gemcitabine for bone cancer treatment. *J. Drug Deliv. Sci. Technol.* **51**, 629–638 (2019).
32. **S.S. Dhaneshwar, K. Mini, N. Gairola, and S.S. Kadam:** Dextran: A promising macromolecular drug carrier. *Indian J. Pharm. Sci.* **68**, 705 (2006).
33. **J.D. Cabral, M. Roxburgh, Z. Shi, L. Liu, M. McConnell, G. Williams, N. Evans, L.R. Hanton, J. Simpson, S.C. Moratti, and B.H. Robinson:** Synthesis, physicochemical characterization, and biocompatibility of a chitosan/dextran-based hydrogel for postsurgical adhesion prevention. *J. Mater. Sci. Mater. Med.* **25**, 2743–2756 (2014).
34. **J. Varshosaz:** Dextran conjugates in drug delivery. *Expert Opin. Drug Deliv.* **9**, 509–523 (2012).
35. **X. Feng, D. Li, J. Han, X. Zhuang, and J. Ding:** Schiff base bond-linked polysaccharide-doxorubicin conjugate for upregulated cancer therapy. *Mater. Sci. Eng. C Mater. Biol. Appl.* **76**, 1121–1128 (2017).
36. **T. Doane and C. Burda:** Nanoparticle mediated non-covalent drug delivery. *Adv. Drug Deliv. Rev.* **65**, 607–621 (2013).
37. **L. Qiu, C.Y. Hong, and C.Y. Pan:** Doxorubicin-loaded aromatic imine-contained amphiphilic branched star polymer micelles: synthesis, self-assembly, and drug delivery. *Int. J. Nanomedicine* **10**, 3623–3640 (2015).
38. **T. Miao, J. Wang, Y. Zeng, G. Liu, and X. Chen:** Polysaccharide-based controlled release systems for therapeutics delivery and tissue engineering: From bench to bedside. *Adv. Sci.* **5**, 700513 (2018).

39. **Y. Zhang, M. Huo, J. Zhou, A. Zou, W. Li, C. Yao, and S. Xie:** DDSolver: An add-in program for modeling and comparison of drug dissolution profiles. *AAPS J.* **12**, 263–271 (2010).
40. **M. Gierszewska-Drużyńska, and J. Ostrowska-Czubenko:** Mechanism of water diffusion into noncrosslinked and ionically crosslinked chitosan membranes. *Prog. Chem. Appl. Chitin Deriv.* **17**, 63–70 (2012).
41. **R.Y. Basha, T.S. Sampath Kumar, and M. Doble:** Dual delivery of tuberculosis drugs via cyclodextrin conjugated curdlan nanoparticles to infected macrophages. *Carbohydr. Polym.* **218**, 53–62 (2019).
42. **International Organization for Standardization. ISO** 10993-5. *Biological Evaluation of Medical Devices – Part 5: Tests for In vitro Cytotoxicity* (ISO, Geneva, 2009).
43. **T.C. Chou:** Theoretical basis, experimental design, and computerized simulation of synergism and antagonism in drug combination studies. *Pharmacol. Rev.* **58**, 621–681 (2006).
44. **W. Song, Z. Tang, M. Li, S. Lv, H. Sun, M. Deng, H. Liu, and X. Chen:** Polypeptide-based combination of paclitaxel and cisplatin for enhanced chemotherapy efficacy and reduced side-effects. *Acta Biomater.* **10**, 1392–1402 (2014).
45. **M. Rahimi, K.D. Safa, and R. Salehi:** Co-delivery of doxorubicin and methotrexate by dendritic chitosan-g-mPEG as a magnetic nanocarrier for multi-drug delivery in combination chemotherapy. *Polym. Chem.* **8**, 7333–7350 (2017).
46. **S.W. Lowe and A.W. Lin:** Apoptosis in cancer. *Carcinogenesis.* **21**, 485–495 (2000).
47. **S.H. Kim and C.C. Chu:** Synthesis and characterization of dextran–methacrylate hydrogels and structural study by SEM. *J. Biomed. Mater. Res.* **49**(4), 517–27 (2000).
48. **Y. Zhang and J. Lu:** A simple method to tailor spherical nanocrystal hydroxyapatite at low temperature. *J. Nanoparticle Res.* **9**, 589–594 (2006).
49. **A.P. Francis, S. Gurudevan, and A. Jayakrishnan:** Synthetic polymannose as a drug carrier: synthesis, toxicity and anti-fungal activity of polymannose-amphotericin B conjugates. *J. Biomater Sci. Polym.* **29**, 1529–1548 (2018).
50. **C.K. Balavigneswaran, S.K. Mahto, B. Subia, A. Prabhakar, K. Mitra, V. Rao, M. Ganguli, B. Ray, P. Maiti, and N. Misra:** Tailored chemical properties of 4-Arm star shaped poly(D, L-lactide) as cell adhesive three-dimensional scaffolds. *Bioconjugate Chem.* **28**, 1236–1250 (2017).